

When Imbalance Comes Twice: Active Learning under Simulated Class Imbalance and Label Shift in Binary Semantic Segmentation

Julien Combes^{1,2[0009-0000-5205-0710]}, Alexandre Derville¹, and Jean Francois Coeurjolly²

¹ Michelin, Clermont-Ferrand, 63000, France

julien.combes@michelin.com alexandre.derville@michelin.com

² Laboratoire Jean Kuntzmann, Grenoble, 38000, France

jean-francois.coeurjolly@univ-grenoble-alpes.fr

Abstract. The aim of Active Learning is to select the most informative samples from an unlabelled set of data. This is useful in cases where the amount of data is large and labelling is expensive, such as in machine vision or medical imaging. Two particularities of machine vision are first, that most of the images produced are free of defects, and second, that the amount of images produced is so big that we cannot store all acquired images. This results, on the one hand, in a strong class imbalance in defect distribution and, on the other hand, in a potential label shift caused by limited storage. To understand how these two forms of imbalance affect active learning algorithms, we propose a simulation study based on two open-source datasets. We artificially create datasets for which we control the levels of class imbalance and label shift. Three standard active learning selection strategies are compared: random sampling, entropy-based selection, and core-set selection. We demonstrate that active learning strategies, and in particular the entropy-based and core-set selections, remain interesting and efficient even for highly imbalanced datasets. We also illustrate and measure the loss of efficiency that occurs in the situation a strong label shift.

Keywords: Active-learning · Machine-vision · Class-imbalance · Label-shift · Domain-adaptation

1 Introduction

In industrial contexts, the collection of substantial datasets to address specific tasks is typically feasible. However, in the context of semantic segmentation for defect detection in quality control, most images are defect free due to the high reliability of production processes. For instance, an automatic visual inspection system (such as described in [14]) placed at the end of a production line is exposed to mostly healthy images. Indeed, manufacturing processes are subject to rigorous quality control policies with the aim of minimising the number of defects along production lines. The process yields a substantial volume of data, yet

only a limited portion is characterised by substantial informational content (in our case, this is evidenced by the presence of segmentation masks). This results in a marked class imbalance, wherein the defect class is noticeably underrepresented in comparison to the background or non-defective regions. This imbalance poses a significant challenge for learning approaches and is particularly critical in active learning settings, where the selection of informative samples might be biased towards the majority class, see e.g. [16].

Active learning. Although substantial quantities of industrial data can be collected, a significant impediment pertains to the necessity for expert annotation, a process that is both costly and time-consuming, yet indispensable for the training of segmentation models. Active learning is proposed as a solution to reduce annotation effort by identifying the most informative samples, thereby allowing accurate models to be trained with minimal labelled data. Despite the fact that pioneering contributions to active learning (AL for short) in image processing emerged over a decade ago [8], there has been a considerable surge in interest in this domain with the advent of sophisticated deep segmentation architectures [13]. In the context of defect detection, it is noteworthy that the majority of images are found to be free of defects. It is important to note that these samples are frequently excluded from training due to the fact that segmentation networks are designed to operate solely on defective samples. In this paper, the investigation focuses on the influence of the proportion of defect-free images present in the unlabelled dataset on the effectiveness of active learning strategies for binary semantic segmentation. Two main frameworks coexist within active learning [17]. The first is the **pool based** AL where we consider two sets of data, a set where the data is labeled and another non-annotated one. In this setting, we consider a specific budget of data (number of unlabelled data that can be labeled) that is queried from the unlabelled pool of data. A statistical model is trained on the newly updated dataset, iterating this process for a predefined number of cycles or until the labeling capacity is exhausted. The second approach is the **stream based** [12] AL where the data to be labeled is selected at the data acquisition time.

The drawback of the pool-based setting is the long-term storage requirement for unlabelled datasets, which can quickly grow in size, particularly in machine vision applications. However, this setting ensures to get the most relevant and informative data to train the model. A balance must be struck between minimizing data storage and preserving potentially informative datasets. In the domain of machine vision applied to quality control, it is imperative to avoid the loss of informative images during the training of deep learning models. This paper, therefore, focuses only on the sensitivity of pool-based AL algorithms.

Class imbalance. The class imbalance in computer vision is dependent on the problem trying to be solved. Indeed, in image classification, each image corresponds to a certain class, so the weights are depending on the number of each image belonging to each class. However, in semantic segmentation, the classi-

fication is done at the pixel level, so we should know what is the number of pixels belonging to each class, which makes it more likely to lead to imbalance. Many approaches exist to tackle the class imbalance problem in the parameters estimation phase such as [3], like oversampling low frequency classes or undersampling frequent classes. In deep-learning the preferred methods rely on tinker with the model loss, by weighting the loss function depending on each class frequency, also known as cost sensitive learning [5]. In the field of image segmentation, novel loss functions have been developed to address the challenges posed by difficult-to-classify pixels. A notable example is the focal loss proposed by [11] which requires prior knowledge of the class distribution and/or tuning hyperparameters. In the context of AL, where the availability of labelled data is limited, it is imperative to retain as much data as possible for the training process. The descriptive analysis of Active Learning on imbalanced data algorithms remains rare. Numerous studies concentrate on AL algorithms that operate on imbalanced datasets [1,22,23] to our knowledge, only one applied those concepts on semantic segmentation [21]. Some research has been conducted into running simulation studies, and we could find one involving synthetic class imbalance in image classification by removing images from certain categories on the CIFARs datasets [4]. However, it is difficult to quantify imbalance in these settings when comparing different levels of imbalance. Indeed, we don't know whether the introduced imbalance is the source of the observed results or whether the same results would have been obtained with other modifications to the distributions. Creating synthetic imbalance in the multiclass setting is challenging.

Label Shift. In industry, most of produced images are healthy and only faulty ones are used for training (i.e. 100% of images in the training set contain defects). Two factors contribute to this circumstance. Primarily, storage capacities are constrained, requiring a preliminary selection of images to be uploaded and subsequently saved for future labeling. Secondly, in the industrial sector, despite the rarity of defects, their identification is of paramount importance. Industries cannot afford leaks that could lead to adverse consequences. Training on primarily faulty data can skew the distribution towards false positive while minimizing leaks. However, once the trained model is deployed, the data generally contains very few faulty images. This difference between the training set and the production set, which is similar to the test set, is addressed in [23]. The authors propose a framework that characterizes label shift across three cases, defined by the distributions of the selected (labeled) data, the unlabelled pool, and the inference (test) data. In this paper, we analyze two cases: (1) the traditional AL setting, where the test distribution matches the unlabelled pool distribution; and (2) an industrially realistic setting, where upstream rules determine which images are stored (to optimize storage), thereby shaping the unlabelled pool, while the test distribution is fixed by the factory/deployment data distribution. In industrial settings, the underlying data distribution is unknown before labeling. Therefore, we seek to guarantee that, under varying levels of class imbalance and label shift, standard AL strategies perform no worse than random sampling.

The rest of the paper is organized as follows. Section 2 presents the setting of pool-based active learning applied to semantic segmentation including main notation used in this manuscript. We also detail the active learning algorithms we consider, provide some implementation details and summarize the criteria we use to compare them. Section 3 is the core of our paper. We propose a simulation study based on two open-source datasets. We specify how we construct, in a fair and reproducible way, datasets for which we control the class imbalance and label shift. Then, we apply the different AL algorithms to these generated datasets, present and discuss the results. A conclusion, providing recommendations and open questions in the context of machine vision, ends this section.

2 Method

2.1 Active learning and semantic segmentation in machine vision

Pool-based AL applied to semantic segmentation in machine vision consists in sequentially labeling a small amount of images extracted from an unlabelled dataset and then train a model based on this subsampled dataset. Let $D^u = \{X_i^u, i \in \mathcal{D}^u\}$ be the set of unlabelled images, where $X_i^u \in \mathbb{R}^{3q}$ are independent RGB images, where q is the number of pixels. It is worth mentioning that D^u could already be a subset of $D^c = \{X_i, i \in \mathcal{D}^c\}$ a set of collected (or acquired) images. Indeed, it is quite common in industrial setting that $\#\mathcal{D}^c$ is so massive that all images cannot be stored and that a preliminary filtering, most often depending on X_i , is performed. In other words, \mathcal{D}^u is to be seen as a random discrete subset of \mathcal{D}^c and $P(i \in \mathcal{D}^u)$ depends on i . Now, that D^u is defined, we assume that each image X_i can be submitted to an oracle or expert who labels the image X_i^u , i.e. defines a mask $Y_i^u \in \{0, 1\}^p$ for any $i \in \mathcal{D}^u$. We further define the random variables $I_i^u = \mathbf{1}(\|Y_i^u\|_1 > 0)$ where $\|z\|_1$ stands for the ℓ^1 -norm of $z \in \mathbb{R}^p$. The variable I_i^u indicates whether a given segmentation mask contains at least one pixel with class 1, i.e. the fact that an image is classified as one containing at least one defect or not. Given \mathcal{D}^u , the unlabelled dataset D^u is characterized by $\pi^u = \sum_{i \in \mathcal{D}^u} P(I_i^u = 1 \mid i \in \mathcal{D}^u) / \#\mathcal{D}^u$ which represents the average proportion of faulty images among D^u .

The AL proceeds as follows. At cycle $j = 0, \dots, J$, we extract a set of images S_j^u from the unlabelled dataset, i.e. a set of indices $\mathcal{S}_j^u \subset \mathcal{D}^u$ with size $\#\mathcal{S}_j^u = B$ called the budget. We form the set $S_j^u = \{X_i^u, i \in \mathcal{S}_j^u\}$. These images are labeled by the expert and the whole is stored in $S_j^\ell = \{(X_i^u, Y_i^u), i \in \mathcal{S}_j^u\}$. The model is then trained on $D_j^\ell = D_{j-1}^\ell \cup S_j^\ell$ (with $D_{-1}^\ell = \emptyset$). The trained model at cycle j , say \hat{f}_j , is directly used to score/predict every image from $D^u \setminus \bigcup_{k=0}^j S_k^u$. The scores or predicted probabilities are denoted by $s_{i,j}^u$ and $\hat{p}_{i,j}^u$ for any $i \in \bigcup_{k=0}^j \mathcal{S}_k^u$. The predicted probabilities or scores (depending on the AL strategy) are then used to extract the next set of images S_{j+1}^u from $D^u \setminus \bigcup_{k=0}^j S_k^u$. The procedure, initialized with \mathcal{S}_0^u randomly selected from $\{1, \dots, \#\mathcal{D}^u\}$, is performed J cycles.

To track the performances of the AL algorithm, we apply the procedure on a test dataset $D^t = \{(X_i^t, Y_i^t), i \in \mathcal{D}^t\}$. In the industrial context, the test dataset is

to be seen as representing model deployment, where the model is applied to real images acquired over time. Thus, in some sense, the way images are included in D^t is the same than the initial ones from D^c , i.e. unlike the set \mathcal{D}^u , there is no reason that $P(i \in \mathcal{D}^t)$ depends on i . The dataset D^t is characterized by $\pi^t = \sum_{i \in \mathcal{D}^t} P(I_i^t = 1) / \#\mathcal{D}^t$ which measures the average proportion of faulty images among D^t . The whole procedure is illustrated in Figure 1

The next section details the simulation setting we consider. We mainly play with the two parameters π^u and π^t . Since we do not model the distribution of $Y_i | X_i$, these probabilities are non-evaluable and we replace them by their empirical versions $(\mathcal{D}^\bullet)^{-1} \sum_{i \in \mathcal{D}^\bullet} \mathbf{1}(I_i^\bullet = 1)$ for $\bullet = u, t$. We abuse notation by still denoting π^u and π^t these quantities. A small value of π^u is related to the concept of **class imbalance**, i.e. D^u contains very few faulty images. The situation $\pi^t = \pi^u$ corresponds to a situation where the test and unlabelled datasets have the same distribution, while the situation $\pi^u >> \pi^t$ reflects that we have more faulty images in the unlabelled dataset than in the test one and illustrates a particular case of the concept **label shift** due to limited storage capacity, where the difference in distribution between the training set (i.e. unlabelled dataset) and the test set ensues from a limited storage constraints which imposes some pre-filtering of D^c .

2.2 Active Learning Algorithms

The focus of this paper is more on the sensitivity of active learning algorithms to class imbalance and label shift than the performances of the algorithm themselves. Hence, we aim to compare two state of the art acquisition functions used in semantic segmentation ([15]) which are the entropy selection [8] and the core-set selection [18]. We also consider the basic strategy consisting in uniform random sampling.

Random Sampling. This strategy is the baseline, where we sample images from the unlabelled dataset according to a uniform distribution.

Entropy Sampling. Semantic segmentation being a collection of classifiers, we can compute the Shannon entropy for each predicted pixel and average them over the full image to get a level of uncertainty for this image. Let \hat{p} be the vectorized predicted probabilities. The average image entropy, in the case of binary semantic segmentation, is then given by $q^{-1}\{\hat{p}^\top \log \hat{p} + (1-\hat{p})^\top \log(1-\hat{p})\}$. This strategy is representative of latent-space *exploitation*, in which the selection process specifically targets the weaknesses of the model. This method, referred to as entropy in the plots, aims to optimize the learning process by strategically choosing samples that are the most difficult for the model. This approach can improve model performance by concentrating on regions of high uncertainty. However, it also has limitations: it may overfit to specific weaknesses and overlook potentially valuable information in areas where the model already performs well. In the context of semantic segmentation in particular, averaging entropy values tends to favour images containing larger defects, as illustrated in Figure 2.

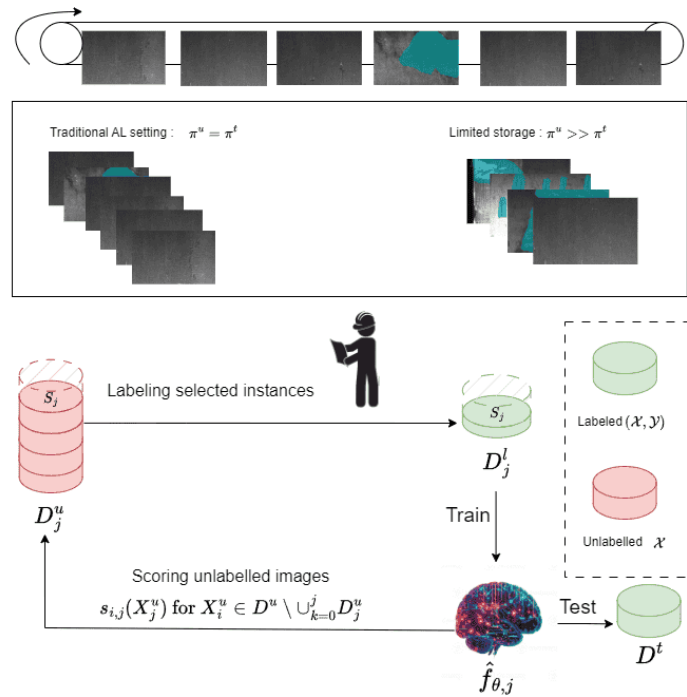


Fig. 1: From top to bottom. (i) Data acquisition: images are collected in the factory according to a production distribution π^t ; (ii) The standard AL setting corresponds to the one where all collected images are stored (situation where $\pi^u = \pi^t$). Due to limited storage capacity, it may happen that only some images are stored according to expert rules (situation $\pi^u \gg \pi^t$). (iii) Active Learning procedure: each cycle j selects a pool of images, S_j^u , from D^u , label selected images (giving rise to S_j^l), train a model on on $D_j^l = D_{j-1}^l \cup S_j^l$ and uses this trained model $\hat{f}_{\theta,j}$ to select most informative images from $D^u \setminus \cup_{k=0}^j D_k^u$ with an acquisition (or score) function s .

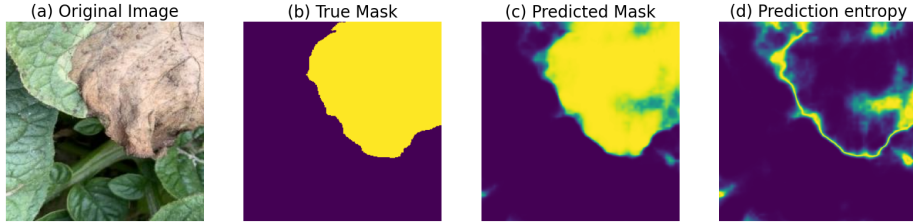


Fig. 2: (a) example on an image from the potato disease dataset. (b) True faulty pixels in yellow. (c) Predicted probabilities for the defect class. (d) Pixelwise Entropy on the prediction of a trained model. Yellow : Faulty, Purple : Healthy. This is done with a model trained on the full patched dataset for illustration purposes.

Core-Set Sampling. For the core-set selection, the algorithm proposed by [18] is considered by using the original Euclidean distance. The embeddings used for the core-set selection are the L^2 -normalized features obtained from the global average pooling of the six multi-scale feature maps produced by the FPN encoder. This strategy focuses on *exploration* of the latent space, aiming to generate images that are highly diverse from one another. The method—referred to as deepcoreset in the next section—builds on the original DeepCore algorithm. By prioritizing diversity in the selected samples, we seek to enhance the model’s capacity to capture a broader range of features and characteristics within the latent space. While this approach can lead to a more comprehensive representation of the dataset, it may also introduce redundancy when the selected diverse samples overlap with regions that are already well understood.

2.3 Implementation details

For this numerical study we consider the simple model for semantic segmentation which is a Feature Pyramid Network [10]. This neural network model is able to extract features of different sizes in images and is pre-trained with the weights of imageNet. The problem is binary semantic segmentation, since each pixel can either be background or defect. The output of the model is a matrix with two channels where each channel represents the probability of each class of being true according to the model. All models are optimized on NVIDIA T4 GPUS with Adam ([9]) a batch size of 52 (Maximum GPU capacity) during 40 epochs with a learning rate of 1×10^{-4} . The loss function we consider is the Combo Loss [20], combination of DiceLoss [19] and Binary Cross entropy Loss computed at the pixel-level and averaged over the whole image. Using multiple losses is quite common in semantic segmentation, see [7]. Let Y and \hat{p} be respectively the vectorized binary mask and predicted probabilities of an image. This loss is

given by

$$\mathcal{L}_{Combo} = \frac{-2\hat{p}^\top Y + S}{(\hat{p} + Y)^\top 1 + S} - \frac{1}{q} \hat{p}^\top \log(\hat{p}) + (1 - \hat{p})^\top \log(1 - \hat{p})$$

where $S \in \mathbb{R}^+$ is a real number used for computational stability, set to 1, as recommended by [19].

2.4 Evaluation Criteria

To understand how AL strategies are affected by class imbalance and/or label shift, we intend (i) to measure the efficiency and the variability of each AL strategy (ii) to understand which type of images from the unlabelled datasets are selected at each cycle. For the task (i), we propose to consider **F1-Score of the faulty class** computed on the test sets. This metric evaluates the model's prediction quality by considering both precision and recall, thereby providing a balance between the two in scenarios where the class distribution is skewed. To measure the variability, we repeat the whole procedure **15 times**, restarting each time with a set S_0^ℓ randomly chosen from D^u . For the task (ii), we evaluate the **proportion of faulty images** selected by each AL strategy and for each cycle. In addition, to have an idea of which images are selected over the 15 repetitions, we construct a score called **uniqueness score** for each cycle, denoted by us_j and given by

$$us_j = \frac{|\cap_{r=0}^R S_{j,r}^\ell| - b}{b(R-1)} \quad (1)$$

where b is the number of images added at each cycle, $R = 15$ is the number of repetitions of the AL procedure per cycle and where $S_{j,r}^\ell$ is the set of images selected and labelled at cycle j for the repetition r . For a given cycle, the score equals 1 (resp. 0) when all selected images are different (resp. similar).

3 Simulation setting, results and conclusion

3.1 Imbalanced dataset construction

To increase robustness of findings, we propose to consider two different open-source datasets. The first one is the *potato diseases dataset* [2] which contains agricultural images of potato leaves. It consists of 5165 3x512x512 RGB images of potato leaves. Each image is accompanied with a segmentation mask that we binarize, where the value 0 means healthy. Given that images are the primary data units rather than individual pixels, we categorize them into 'healthy images' when they contain no faulty pixels, and 'faulty images' in the opposite case. Note that all masks contain at least one non-zero pixel. The second considered dataset is the *severstal dataset* [6] which is an open machine vision dataset with semantic segmentation labels of defects on metal plates. This dataset contains 18,074 256x1600 grey-scale images with 6,640 faulty images (37%), the targets are binarized as well.

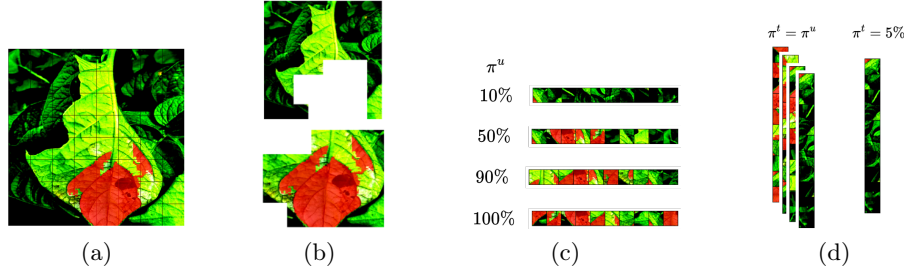


Fig. 3: (a) Original Image 512x512, Every image contains defective pixels (b) Patchification into 256x256 patches. This creates two sets of images : the first one composed of the healthy pixels and the second one with the defects only (c) Synthetic Class imbalance by randomly sampling each set of images according to a predefined proportion of defects (d) Test set distributions under AL assumption and industrial case fixed at 5%

In order to create datasets with different values of π^t and π^u and make the findings comparable between both datasets, we decide not to work on the full images but on patches of 3x256x256. After patchifying the potato diseases training dataset we end up with 25,788 smaller images. 20,341 of them are faulty and 5,447 are healthy, which is about 79% of faulty images. The severstal dataset contains greyscale image with dimension 256x1600, we patch each image into 256x400 smaller images. We end up with 43,048 patches with 9,358 faulty ones. (22%). Since we aim to construct subsets with π^u ranging from 0% to 100%, we set the size of the unlabelled subset to 4300 i.e. $\approx 80\%$ of the maximal possible dataset size (5,447). The datasets are constructed randomly by sampling the required number of items from each training or test set to reach any desired value of π^u and π^t (see Figure 3 with one image as an example). To investigate the class imbalance sensitivity, we let $\pi^u = 10\%, 50\%, 90\%, 100\%$. The label shift sensitivity is controlled by the difference between π^u and π^t . We consider $\pi^t = \pi^u$ (no label shift) and $\pi^t = 5\% < \pi^u$. We run this experiment for $J = 10$ cycles, so that $\#\mathcal{D}_j^u / \#\mathcal{D}^u = 2\%, 4\%, \dots, 20\%$. Each cycle is repeated 15 times. We report the F1-score with uncertainty bands represented by the interquartile range. Figures 4 summarises the main results.

3.2 Results

Figures 4 constitute the core of this paper and summarize our findings for the two potato diseases and severstal datasets. The figure reports F1-scores defect in terms of the budget (percentage of the size of the unlabelled dataset) for ten cycles, 15 replications per cycle, three active learning strategies and the two settings $\pi^u = \pi^t$ (no label shift) and $\pi^t < \pi^u$ and this for different values of π^u .

We first comment Figure 4 (a) (potato diseases dataset). First of all, as expected, the higher the budget the higher F1-scores and this holds for all AL

strategies and the two situations. Consider the situation $\pi^t = \pi^u$ (first row of Figure 4). Entropy and deep core-set based methods clearly outperform the naive random sampling. The observed differences, with the naive random sampling method, are larger in the two following situations: (i) first, when datasets contain very few faulty images, i.e. for highly class-imbalanced unlabelled datasets; (ii) second, when the budget is moderate. Finally, it is worth mentioning that the variability, represented by the interquartile pointwise bands, decreases when the budget or π^u increases, as one could expect. Let us also add that the entropy based AL strategy provides the most stable results. In presence of label shift in the data generation (second row of Figure 4), the F1-scores still increase with the budget in all considered cases. However, first, the differences between the three AL strategies are less clear especially when $\pi^u >> \pi^t$. Second, given a value of π^u , we observe that F1-scores are reduced when $\pi^t = 5\%$ compared to the 'no label shift situation'. For example for a budget of 10% and for the entropy based method, the loss of F1-score in percentage equals approximately 16%, 50%, 63% and 69% when $\pi^u = 10\%, 50\%, 90\%$ and 100% . Third, all methods become less stable than when $\pi^u = \pi^t$. Unlike the 'no label shift' situation, the interquartile pointwise bands do not significantly decrease with the budget or π^u .

The results for the Severstal dataset, shown in Figure 4(b), exhibit greater variability (as indicated by wider interquartile pointwise bands), and the overall performance (F1-scores) is slightly lower than for the first dataset. This can be attributed to the higher complexity of the images under analysis. Nevertheless, most of the observations made for the potato diseases dataset still apply to the Severstal dataset, which, in our view, reinforces the usefulness and reproducibility of the present study.

One may wonder which types of images are selected throughout the cycles of the different active learning (AL) strategies. Figure 5 provides insights for the potato disease dataset, and similar observations hold for the Severstal dataset. Overall, Figure 5 shows that, unlike random sampling, both the entropy-based and core-set strategies tend to select a higher proportion of faulty images than the underlying proportion π^u . This behavior is particularly pronounced for the entropy-based method, which selects on average 40% faulty images, even though the unlabeled dataset contains only 10% of such images. Although these two methods share this tendency, they differ in the specific images they select. The uniqueness scores obtained with the deep core-set strategy are much more variable than those of the entropy-based strategy, further illustrating the notions of exploration and exploitation associated with these two approaches, respectively.

3.3 Conclusion

This study demonstrates that AL improves label efficiency and inference performance over random sampling across a range of class-imbalance and label shift regimes, with the most pronounced benefits at moderate to high imbalance and very moderate label shift. Beyond F1-scores, AL-trained models exhibit greater stability. Indeed, they are less dependent on the initial labeled set and rarely

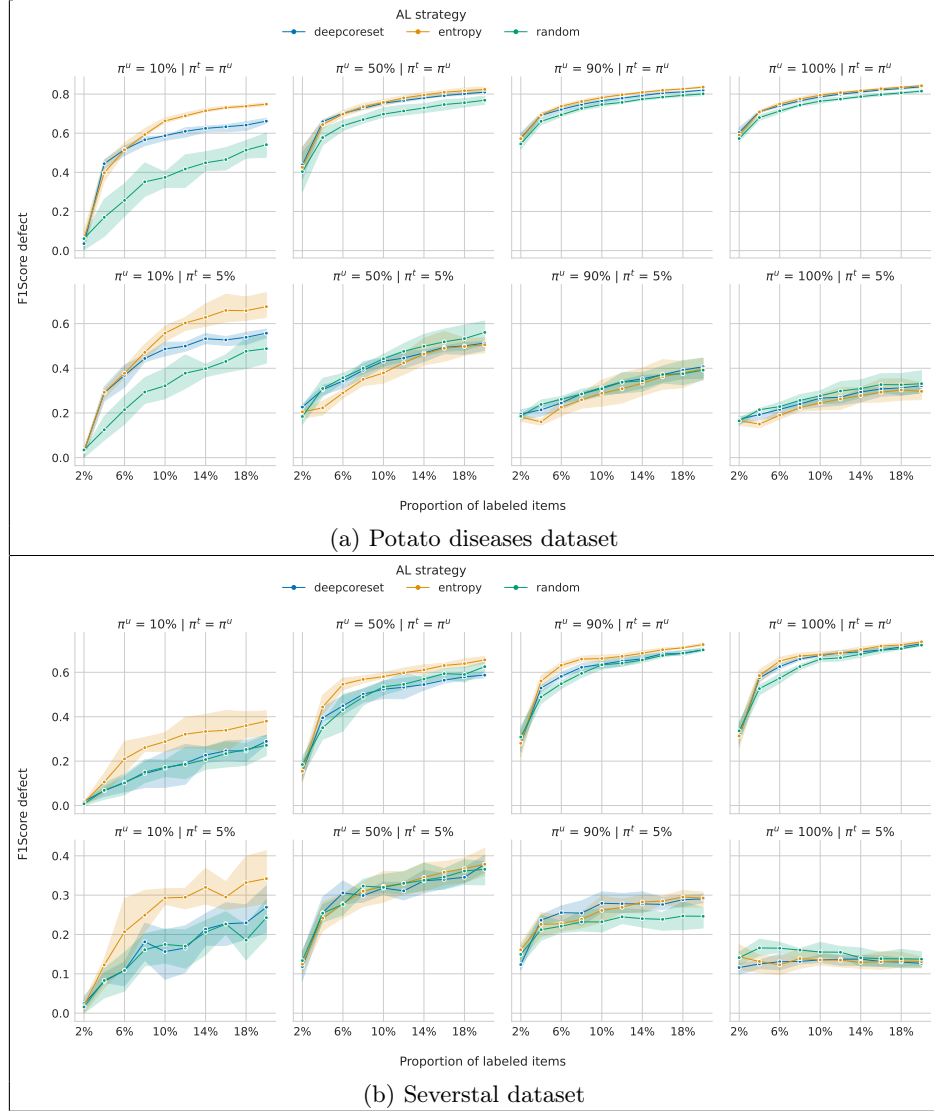


Fig. 4: Test F1-scores for the potato diseases dataset, (a), and for the severstal dataset, (b). For each dataset, scores are based on 10 AL cycles from 2% to 20% of the size of the unlabelled dataset. The solid line (resp. bands) represents (resp. represent) the mean curve (resp. interquartile range pointwise bands) obtained over 15 repetitions. The upper row are the results on the test set following the same distribution of the unlabelled dataset (no label shift). The bottom row depicts the performances of the same model but on a test set with a different distribution (where only 5% of images contain faulty pixels).



Fig. 5: (a) Proportion of faulty images selected at each cycle for the potato diseases dataset. (b) Uniqueness scores for the potato disease dataset defined by (1). Remind that a uniqueness score of 0.5 means that among all images selected at cycle j , half of them are unique.

degrade as more labeled data are added. By systematically prioritizing informative samples from large unlabelled pools, AL mitigates the operational burden of annotating predominantly non-defective images and reduces sensitivity to unlabelled pool composition. While AL's advantage narrows under severe pool target distribution mismatch, our results indicate that AL remains at least non inferior to random selection and often superior when the deployment prevalence is reasonably aligned. Overall, AL offers a practical, scalable pathway to robust semantic segmentation in machine vision, particularly in domains characterized by substantial class imbalance and abundant unlabelled data.

Data availability statement

The two datasets used in this paper are open-source at the following URLs :

The potato disease dataset can be downloaded here https://universe.roboflow.com/anup-kaygm/potato_disease-binb3.

The severstal dataset can be downloaded here <https://www.kaggle.com/c/severstal-steel-defect-detection>.

The code is available on this repository : <https://github.com/JulienStats/WhenImbalanceComesTwice>

References

1. Aggarwal, U., Popescu, A., Hudelot, C.: Active Learning for Imbalanced Datasets. In: 2020 IEEE Winter Conference on Applications of Computer Vision (WACV). pp. 1417–1426 (Mar 2020). <https://doi.org/10.1109/WACV45572.2020.9093475>
2. Anup: Potato_disease Dataset (Jun 2024)
3. Buda, M., Maki, A., Mazurowski, M.A.: A systematic study of the class imbalance problem in convolutional neural networks. *Neural Networks* **106**, 249–259 (Oct 2018). <https://doi.org/10.1016/j.neunet.2018.07.011>
4. Choi, J., Yi, K.M., Kim, J., Choo, J., Kim, B., Chang, J.Y., Gwon, Y., Chang, H.J.: VaB-AL: Incorporating Class Imbalance and Difficulty with Variational Bayes for Active Learning (Dec 2020). <https://doi.org/10.48550/arXiv.2003.11249>
5. Elkan, C.: The foundations of cost-sensitive learning. In: Proceedings of the 17th International Joint Conference on Artificial Intelligence - Volume 2. pp. 973–978. IJCAI'01, Morgan Kaufmann Publishers Inc., San Francisco, CA, USA (Aug 2001)
6. Grishin, A.: Severstal: Steel defect detection (2019), <https://kaggle.com/competitions/severstal-steel-defect-detection>
7. Jadon, S.: A survey of loss functions for semantic segmentation. In: 2020 IEEE Conference on Computational Intelligence in Bioinformatics and Computational Biology (CIBCB). pp. 1–7 (Oct 2020). <https://doi.org/10.1109/CIBCB48159.2020.9277638>
8. Joshi, A.J., Porikli, F., Papanikolopoulos, N.: Multi-class active learning for image classification. In: 2009 IEEE Conference on Computer Vision and Pattern Recognition. pp. 2372–2379 (Jun 2009). <https://doi.org/10.1109/CVPR.2009.5206627>
9. Kingma, D.P., Ba, J.: Adam: A Method for Stochastic Optimization (Jan 2017). <https://doi.org/10.48550/arXiv.1412.6980>

10. Lin, T.Y., Dollár, P., Girshick, R., He, K., Hariharan, B., Belongie, S.: Feature Pyramid Networks for Object Detection (Apr 2017). <https://doi.org/10.48550/arXiv.1612.03144>
11. Lin, T.Y., Goyal, P., Girshick, R., He, K., Dollár, P.: Focal Loss for Dense Object Detection (Feb 2018). <https://doi.org/10.48550/arXiv.1708.02002>
12. Lugofer, E.: On-line active learning: A new paradigm to improve practical use-ability of data stream modeling methods. *Information Sciences* **415–416**, 356–376 (Nov 2017). <https://doi.org/10.1016/j.ins.2017.06.038>
13. Ma, S., Wu, H., Lawlor, A., Dong, R.: Breaking the Barrier: Selective Uncertainty-based Active Learning for Medical Image Segmentation (Jan 2024). <https://doi.org/10.48550/arXiv.2401.16298>
14. Mignot, Thomas and Ponchon, Francois and Derville, Alexandre and Duffner, Stefan and Garcia, Christophe: An automatic inspection system for the detection of tire surface defects and their severity classification through a two-stage multi-modal deep learning approach. *Journal of Intelligent Manufacturing* (May 2024). <https://doi.org/10.1007/s10845-024-02378-3>
15. Mittal, S., Niemeijer, J., Schäfer, J.P., Brox, T.: Best Practices in Active Learning for Semantic Segmentation. In: Köthe, U., Rother, C. (eds.) *Pattern Recognition*. pp. 427–442. Springer Nature Switzerland, Cham (2024). https://doi.org/10.1007/978-3-031-54605-1_28
16. Pop, Remus and Fulop, Patric: Deep ensemble bayesian active learning : Addressing the mode collapse issue in monte carlo dropout via ensembles (Nov 2018). <https://doi.org/10.48550/arXiv.1811.03897>
17. Ren, P., Xiao, Y., Chang, X., Huang, P.Y., Li, Z., Gupta, B.B., Chen, X., Wang, X.: A Survey of Deep Active Learning (Dec 2021). <https://doi.org/10.48550/arXiv.2009.00236>
18. Sener, O., Savarese, S.: Active Learning for Convolutional Neural Networks: A Core-Set Approach (Jun 2018). <https://doi.org/10.48550/arXiv.1708.00489>
19. Sudre, C.H., Li, W., Vercauteren, T., Ourselin, S., Cardoso, M.J.: Generalised Dice overlap as a deep learning loss function for highly unbalanced segmentations. vol. 10553, pp. 240–248 (2017). https://doi.org/10.1007/978-3-319-67558-9_28
20. Taghanaki, S.A., Zheng, Y., Kevin Zhou, S., Georgescu, B., Sharma, P., Xu, D., Comaniciu, D., Hamarneh, G.: Combo loss: Handling input and output imbalance in multi-organ segmentation. *Computerized Medical Imaging and Graphics* **75**, 24–33 (Jul 2019). <https://doi.org/10.1016/j.compmedimag.2019.04.005>
21. Yuan, X., Wang, S., Qu, T., Feng, H., Liu, P., Zeng, J., Chen, X.: Learning the hard-to-learn: Active learning for imbalanced datasets in data-centric tunnel engineering. *Computers and Geotechnics* **174**, 106629 (Oct 2024). <https://doi.org/10.1016/j.compgeo.2024.106629>
22. Zhang, J., Katz-Samuels, J., Nowak, R.: GALAXY: Graph-based Active Learning at the Extreme (May 2022). <https://doi.org/10.48550/arXiv.2202.01402>
23. Zhao, E., Liu, A., Anandkumar, A., Yue, Y.: Active Learning under Label Shift. In: *Proceedings of The 24th International Conference on Artificial Intelligence and Statistics*. pp. 3412–3420. PMLR (Mar 2021)